Induced Seismicity within Geological Carbon Sequestration Projects: Maximum Earthquake Magnitude and Leakage Potential from Undetected Faults

Alberto Mazzoldi[1]*, Antonio P. Rinaldi[1], Andrea Borgia[1], Jonny Rutqvist[1]

[1] Lawrence Berkeley National Laboratory, Earth Sciences Division, 1 Cyclotron Road, Berkeley, USA

*Corresponding author

Tel.: +1-510-486-6878

E-mail address: amazzoldi@lbl.gov

ABSTRACT

With developing countries strongly relying on fossil fuels for energy generation, geological carbon sequestration (GCS) is seen as a candidate for large reductions in CO_2 emissions during the next several decades. GCS does, however, raise some safety concerns. Specifically, it has been associated with induced seismicity, as a result of pressure buildup arising from prolonged CO_2 injection in GCS projects. This seismicity is a delicate issue for two main reasons. First, over a short time scale, deformation of rock could release seismic energy, potentially affecting surface structures or simply alarming the population, with negative consequences for the social acceptance of this kind of project. Second, over a longer time scale, activated faults may provide preferential paths for CO_2 leakage out of reservoirs. While known major faults intersecting target aquifers can be identified and avoided during site screening, the same might not be true for faults that are not resolvable by geophysical surveys. In this study, we use geological observations and seismological theories to estimate the maximum magnitude of a seismic event that could be generated by a fault of limited dimensions. We then compare our estimate with results of geomechanical simulations that consider faults with different hydrodynamic and geomechanical characteristics. The coupled simulations confirm the notion that the tendency of faults to be reactivated by the pressure buildup is linked with the *in situ* stress field and its orientation relative to the fault. Small, active (critically stressed) faults are capable of generating sufficiently large events that could be felt on the surface, although they may not be the source of large earthquakes. Active, relatively permeable faults may be detrimental concerning the effectiveness of a storage project, meaning that they could be preferential pathway for upward CO_2 leakage, although minor faults may not intersect both CO_2 reservoirs and shallower potable aquifers.

Keywords

Undetected faults; Transmissivity; Periodic Flow; Induced Seismicity; Leakage; Carbon Sequestration

Nomenclature

C	*Rock Cohesion (GPa)*
p	*Pore pressure (GPa)*
P	*Pressure (e.g. CO_2 pressure) (GPa)*
T	*Temperature (^oC)*
t_F	*Fault zone thickness (m)*
t_r	*Time after injection starts at which the fault slips (d)*
M	*Earthquake magnitude*
M_0	*Seismic moment (N m)*
D	*Maximum fault displacement (m)*
D_{SING}	*Average slip on the fault plane during a single event (m)*
L	*Length of the fault surface (diameter if considering elliptic features) (m)*
A	*Areal extent of the fault surface (m^2)*
k_{Aq}	*Permeability of the target aquifer (m^2)*
k_{Cap}	*Permeability of cap-rock (m^2)*
k_F	*Fault permeability (m^2)*
$k_{F\text{-}Aq}$	*Fault permeability when crossing the aquifer (m^2)*
$k_{F\text{-}Cap}$	*Fault permeability when crossing the cap-rock (m^2)*
σ_1	*Principal stress vector (GPa)*
σ_2	*Intermediate stress vector (GPa)*
σ_3	*Least stress vector (GPa)*
σ_H	*Horizontal stress in a 2D simulation (GPa)*
σ_V	*Vertical stress in a 2D simulation (GPa)*
σ_n	*Stress component acting normal to a plane (GPa)*
τ	*Stress component acting parallel to a plane (GPa)*
σ_{eff}	*Effective normal stress on a plane (= σ_n- p) (GPa)*
μ	*Coefficient of friction*
η	*Shear modulus*
GCS	Geological Carbon Sequestration
SGR	Shale Gouge Ratio

1 Introduction

The risk of induced seismicity is a general concern for geological carbon sequestration (GCS) projects, owing to the large-scale pressurization resulting from CO_2 injection (e.g., Oldenburg, 2007; Shapiro et al. 2007; Cappa & Rutqvist, 2011a). This induced seismicity remains a major issue for public acceptance of GCS projects located near active, potentially seismic faults: project proponents and regulators inevitably must face this concern. The possibility exists that such induced seismicity may also result from undetected sources: i.e., faults that were not recognized during the site-screening phase of the project. While it is already known how to evaluate seismic hazard for known faults (e.g., Kanamori, 1977; Wells & Coppersmith, 1994; Abercrombie, 1995), the potential for induced seismicity due to undetected faults has not been thoroughly studied.

It has long been recognized that increasing pore pressure reduces the stress normal to the fault surface, thereby reducing fault strength (Terzaghi and Peck, 1948). That is:

$$\tau = C + \mu(\sigma_n - p) \tag{1}$$

where τ is shear stress, C is cohesion, μ is coefficient of friction, σ_n is normal stress, and p is pore pressure. Thus, by raising pore pressure, the effective normal stress on a pre-existing fault surface ($\sigma_{eff} = \sigma_n - p$) is reduced, making it possible for fault reactivation to occur at a level of shear stress at which fault slip, and consequent energy release, would normally not occur (Zoback & Zinke, 2002; Figure 1).

In hydrocarbon fields, fluid injection is a tested practice to increase pore pressure and consequent hydrocarbon production. This technique has in rare cases resulted in the occurrence of major induced seismic events (a summary can be found in Rutqvist & Stephansson, 2003), but, when induced seismicity has occurred, it has caused significant

social anxiety (Dost & Haak, 2007; Majer et al., 2007), even when ground motion was not severe. Therefore, within GCS projects, induced seismicity is of concern especially when dealing with public acceptance of the technology (Oldenburg & Birkholzer, 2010). The cancellation of the GCS experimental project by Shell in Barendrecht, NL, is one of several such instances (Pals, 2010). A magnitude 3.4 event induced by fluid injection at 3 km depth forced the shutdown of the Basel (Switzerland) Hot Dry Rock geothermal project (Dannwolf & Ulmer, 2009).

To ensure better distribution of information to the public and more widespread acceptance of the technology, local governments will likely demand quantitative evaluations of seismic hazards and risks caused by GCS operations. In this regard, the question to be answered is: what would be the maximum earthquake magnitude potentially induced by any particular CO_2 storage operation?

Studying induced seismicity near Denver during the Rocky Mountains Arsenal deep well injection, McGarr (1976) found how the sum of the seismic moments during the three years of injection (1962-1965) can be related to the amount of fluid injected during the same period (McGarr, 1976). Shapiro et al. (2007; 2010) attempted to infer earthquake magnitude during fluid injection by studying how these magnitudes are related to size, distribution, and frequency of pre-existing rock discontinuities, and to injection pressures. They found that the number of earthquakes greater than a given magnitude increases with increasing injection pressure. Shapiro et al. (2010) introduced a "*seismogenic index*" which is linked to the expected level of seismic activity at a given fluid injection site, independent of injection parameters. Cappa and Rutqvist (2011 a, b) analyzed theoretical case studies of seismic energy releases in response to fault slip. Their work focused on major faults with length $L > 2$ km and large offsets.

In the context of mitigating climate change, large amounts of CO_2 need to be injected in target formations (brine aquifers or depleted oil and gas reservoirs), involving areas that could be significantly larger than, say, 10 km in radius (Birkholzer & Zhou, 2009; Pruess, 2003; Court, 2011). Such injections may be located away from known major faults or, if major faults are present, seismic hazard could be reduced by, for instance, production of brine (e.g. Court et al., 2011). Here, we present a method for inferring earthquake magnitudes induced by the activity of minor faults that may remain undetected through both geological and geophysical investigations during the GCS site-screening phase (Figure 2). In fact, it is likely that, over the vast magnitude required for GCS, undetected faults will be intercepted by the pressure-buildup fronts developed during CO_2 injection at various sites.

In this paper, we first provide a review of fault hydrodynamic properties that could influence fluid accumulations. Then, we describe how small faults may influence reservoir strain under regional extension, in order to give an estimate of maximum size of undetected faults. We calculate expected earthquake magnitudes for these faults using empirical magnitude-versus-size relationships. Finally, we compare these results with TOUGH-FLAC (Rutqvist et al., 2002) numerical models of coupled fluid flow and rock mechanics during CO_2 injection, for different hydrodynamic properties of, and stresses acting on, small, potentially undetectable faults.

2 Hydrodynamic Properties of Faults

In a GCS project, CO_2 is injected into a permeable formation, typically sandstone or carbonate, overlaid by a less permeable cap rock, such as shale or anhydrite, that inhibits upward migration of CO_2. During CO_2 injection, native pore fluid(s) within the porous medium are displaced by the injected CO_2 either laterally (e.g. Nicot, 2008) or vertically (e.g., Birkholzer et al., 2011; Oldenburg & Rinaldi, 2011). Pressure perturbations will travel more

rapidly and extend to distances much greater than the CO_2 plume itself (e.g., Zhou and Birkholzer, 2010). Therefore, faults that cannot be resolved by standard seismic imaging can potentially be encountered at any distance from the injection well by the advancing pressure-buildup front.

2.1 Fault-normal Transmissivity

In oil and gas reservoirs, faults usually act as barriers of different strength to the horizontal and vertical flow of hydrocarbon. For production modeling, specific fault-zone hydraulic properties are incorporated into flow simulators using transmissivity multipliers derived from known rock properties, as well as from estimations of damage-zone permeability and thickness (Manzocchi et al., 1999; Yielding et al., 1997). Different methodologies are also used for predicting fault sealing potential within sandstone/shale sequences (e.g., Bouvier et al., 1989; Antonellini & Aydin, 1994). One such methodology is based on the Shale Gouge Ratio (SGR; Yielding et al., 2010). This methodology uses the average clay content of the layers that have slipped past each other on the opposite side of a fault in order to evaluate fault-gouge composition (Figure 3). Clay minerals provide sealing properties to a fault when they are in excess of 15-20% in the gouge; i.e., SGR ≥ 0.15-0.2 (e.g., Antonellini & Aydin, 1994). Fault-gouge permeability data from reservoir and outcrop samples suggest a general decrease in fault-zone permeability with increasing shale content in the faulted rock-sequence, and large variations in permeability at any given shale content. The higher the fault throw the finer the fault breccia and the lower the fault zone permeability. Child et al. (2009) and Manzocchi et al. (2010) relate fault-gouge thickness to fault throw in subsurface faults. Figure 4 summarizes data of fault properties as a function of SGR and fault throw. These data suggest variations of at least two orders of magnitude in determining the fault hydrodynamic properties.

2.2 Fault-parallel Permeability and Fault-constrained Hydrocarbon Accumulations

Fault-zone porosity studies, measured flow rates, large differences in fluid potentials of juxtaposed layers, and fault-bounded hydrocarbon accumulations, all suggest that fault zones are not efficient means for the vertical transfer of fluid. On the other hand, fault-zone mineralization, lowered fluid potentials, and thermal and salinity anomalies along fault zones are evidence of faults acting as preferential paths for vertical fluid migration (Hooper, 1991 and references therein). In the past, it was argued that the sealing or non-sealing capacity of a fault depended solely upon the permeability of the fault-gouge zone, and that vertical flow was largely dominated by Darcy's law within the gouge matrix (e.g., Smith, 1966). However, when permeability is very low, as in shale, and capillary pressure becomes extremely high (as in the case of two-phase CO_2 and brine flow), different mechanisms, such as fracture or fault-slip enhanced permeability, must provide preferential pathways for fluid migration (Finkbeiner et al., 2001).

Barton et al. (1995) present strong evidence, from wells drilled in crystalline rock, that faults optimally oriented for shear failure (critically stressed) have increased permeability and conduct fluid along their planes. Non-critically stressed faults, in contrast, appear to provide no fluid migration pathways. Hooper (1991) presents the concept of periodic fluid flow along growth faults within sedimentary basins, for which fluid motion is discontinuous, being restricted in time and space: when faults are active they concentrate fluid flow while, when inactive, flow becomes restricted. This concept of periodic flow is similar to Sibson's fault-valve behavior (Sibson, 1990), but, while the latter is equally valid for different tectonic environments, the former focuses on extensional environments, which are of particular interest for GCS operations, a significant fraction of which are likely to be sited in settings with extensional stress regimes.

Sedimentary basins form in areas of rapid terrigenous sedimentation and subsidence. They are most often characterized by normal faulting, where the overburden stress represent the maximum principal stress. Pore pressures in compacting shales are expected to be higher than in the interbedded sandstone layers, because of their low permeability and consequent poor drainage of connate water. When shales become juxtaposed with sandstone layers across faults, ideal structural traps for hydrocarbons may be formed (Finkbeiner et al., 2001; Yielding et al., 2010). In these situations, the sealing capacity of the fault plane at the top of and along the sand layer dictates the thickness of hydrocarbons that can be supported by the trap: the pressure at the top of the sandstone can potentially be higher than that in the shale above. In a GCS project, during injection near an undetected fault, the potential pore-pressure buildup aside the fault in the injection zone would gradually increase, reducing the effective stress normal to the fault surface (Equation 1), eventually leading to fault slip at the top of the permeable layer. In turn, fault slip and transient permeability increase would induce fluid migration, pore pressure reduction and system re-equilibration.

2.3 Fault Activity and Gas Leakage during Earthquakes

The concept of periodic flow along faults, applied predominantly to compressional tectonic environments (cf. Sibson, 1990), is in principle able to explain gas concentration anomalies (mainly Radon and CO_2) in proximity to the outcrops of active faults, before the occurrence of major natural earthquakes (cf. Chyi et al., 2005; and Singh et al., 2010). Radon (and CO_2) anomalies have been used for potential earthquake predictions since the early 1970s (Ulomov & Mavashev, 1967; Talwani et al., 1980; Kumar et al., 2009). The emissions of these gases are characteristic of active faults, and are a function of fluid availability and tectonic setting (Richon et al., 2010; Mazzoldi, 2004). However, the presence of soil and sediments covering fault outcrops at the surface frequently inhibits the detection of anomalies (Richon et al., 2010).

It is not yet clear whether an anomaly can always be correlated to a major earthquake, as the stress accumulation causing the anomaly may be released aseismically or through many minor events (e.g., Friedmann, 2011), complicating the process of issuing warnings to the public. In April 2009, a researcher detected high fluxes of radon and CO_2 near outcrops of a normal fault that, a few days later, generated a magnitude 6.3 earthquake, with more than 300 fatalities, in the L'Aquila region (Central Italy; EERI, 2009). The study of radon fluxes from the ground cannot reliably be used as an earthquake predictor, although if an anomaly is detected in an area with a known major fault during a known active phase, alerting appropriate government agencies appears to be a useful cautionary measure. In relation to CO_2 injection and storage, observations of leaking gases before or during earthquakes may provide additional evidence for increased fault permeability and reactivation (seismic or aseismic).

3 Faults Size, Areal Distribution, and Seismic Potential

Small faults by far outnumber large faults, with the areal density of fault size generally described by power-law relationships (Gauthier & Lake, 1993; Torabi & Berg, 2011). Through the study of exposed normal faults in outcrops of Cretaceous carbonates in Texas, Morris et al. (2010) found that there is a correlation between fault frequency and bulk extensional strain. In particular, the largest 30% of a total fault population accommodates more than 70% of total extension (Figure 5). Similar power-law relationships describe fault-size frequency in reservoirs of different lithology (e.g., Hesthammer & Fossen, 1997; Torabi & Berg, 2011). These relationships can support predictions of small-faults distribution, density, size and displacement (Morris et al., 2010; Ferrill & Morris, 2003).

3.1 Dimensions of Seismically Undetected Faults

Field observations indicate that there is a correlation between the maximum amount of shear displacement on a fault (*D*) and the length of the fault trace (*L*) (Cowie and Scholz, 1992; Dowrick and Rhoades, 2004; Ferrill et al., 2008; Schlische et al., 1996). Within a particular setting, faults have consistent *D/L* ratios, suggesting that they are scale-invariant (*D/L* is constant) (Dawers et al., 1993; Kim & Sanderson, 2005). Empirical studies show how *D/L* ratios of normal faults, regardless of rock type, range primarily between 10^{-1} and 10^{-2} (Kim & Sanderson, 2005; Schultz & Fossen, 2002), depending on the ratio between rock yield strength and shear modulus (Gupta & Scholz, 2000). Therefore, these ratios are characteristic of geo-dynamical setting and site history (Dowrick and Rhoades, 2004).

Seismic reflection surveying is considered to be unable to resolve faults with $D \leq 10$ m (Gauthier & Lake, 1993; Kim & Sanderson, 2005). Consequently, in order to evaluate a worst-case scenario for seismic energy release, the vertical extent *L* of the largest undetected fault, derived from a low *D/L* ratio ($=10^{-2}$), is $L = 10^3$ m. In turn, fault dimensions and "singular event" displacement determine the magnitude of potential seismic events (as explained in the following section). Due to seismic data quality, in the case of older surveys, the 'undetected faults' could actually be larger than what we have estimated above. In fact, a major undetected, buried (not reaching the surface) fault is thought to have been responsible for the 1994 Northridge 6.7 magnitude earthquake in Southern California (Chavez-Perez & Louie, 1997).

3.2 Magnitude-versus-size Formulas and Events Induced by Non-detectable Faults

Earthquake magnitudes and intensities are correlated with fault rupture parameters such as rupture area and displacement (Bath, 1981; Giampiccolo et al., 2007; Iida, 1959). Accordingly, paleoseismic and geologic studies of active faults focus on evaluating these

parameters, which are then translated into estimates of earthquake intensities (Abercrombie, 1995; Shaw, 2009).

The seismic moment (M_0) of an earthquake is defined as a function of fault rupture (Hanks & Kanamori, 1979) by

$$M_0 = \eta D_{SING} A \quad (2),$$

where η is the shear modulus of the host rock, D_{SING} is the average displacement across the fault surface during a single event, and A is the area of the fault-surface rupture. In turn, M_0 is directly related to magnitude (M) (Wells & Coppersmith, 1994) by

$$M = \frac{2}{3}\left[\log_{10}(M_0) - 9.1\right] \quad (3).$$

Therefore:

$$M = \frac{2}{3}\left[\log_{10}(\eta D_{SING} A) - 9.1\right] \quad (4).$$

Ferrill et al. (2008) explored the D_{SING}/L ratio for single earthquake events induced by normal faults with a rupture length range of 10^2–10^3 m, in a data set from the Newberry Springs Fault Zone, USA. They found that ruptures along this fault zone have an average $D_{SING}/L = 8 \times 10^{-5}$. If we can approximate the average displacement-to-length ratio during single events for the faults under consideration to be 10^{-4}, ruptures with $L = 10^3$ m have $D_{SING} = 0.1$ m. Substituting these values into Equations (2) and (4), we find:

$M_0 = 3 \times 10^9 \times 0.1 \times \pi \times 500^2 = 2.35 \times 10^{14}$ (Nm)

$M = 3.59$

where 3×10^9 is the shear modulus (Pa), 0.1 (m) is the single-event fault displacement, and 500 is the radius of the fault ($r = L/2$, m), which for simplicity is assumed to be circular.

4 Coupled Fluid Flow and Geomechanical Modeling in 2D

The relative motion of the fault walls is primarily influenced by the local stress conditions—that is, by the values of the principal stresses $\sigma_1 > \sigma_2 > \sigma_3$. For our 2D simulations of normal faulting, we assume that σ_1 and σ_3 are on the X/Z reference plane and equal to the vertical (σ_V) and horizontal (σ_H) stresses, respectively. The values of the stress components normal (σ_n) and parallel (shear, τ) to the fault plane, defining the stress conditions at the fault surface, are given by:

$$\tau = \frac{\sigma_1 - \sigma_3}{2} \sin 2\delta \tag{6}$$

$$\sigma_n = \frac{\sigma_1 + \sigma_3}{2} - \frac{\sigma_1 - \sigma_3}{2} \cos 2\delta \tag{7}$$

where δ is the angle between the fault plane and the direction of σ_1. The ease of reactivation of existing faults varies with their specific orientation relative to the local 3D stress field (e.g., Sibson, 1990): the generalization of these equations to this case is not difficult, but for the purpose of this study our 2D formulation is considered sufficient. 2D stress analysis and strain simulation allow us to neglect the effect of σ_2 on the overall strain. In order to estimate the maximum pressure buildup sustainable by faults not favorably oriented for slippage, the intermediate stress is accounted for by increasing the value of the stress normal to the fault surface (see below).

We analyze the effects of varying permeability and mechanical conditions at the fault plane (initial regional state of stress, σ_H/σ_V) on the total amount of slip on the surface in order to estimate the energy released and magnitude of the seismic event as a response to the increase in pore pressure. For this analysis, we use a coupled implementation of the TOUGH fluid-flow simulator and the FLAC geo-mechanical simulator (Rutqvist et al., 2002; Cappa and Rutqvist, 2011a).

Common to all the simulations is a 1 km long normal fault crossing the target GCS reservoir

near its mid-length, at a depth of about 1,500 m and at a horizontal distance from the injection well of 500 m; the fault is inclined at 10° with respect to vertical (Figure 6). The idealized trap-system is characterized by 150 m thick shale with permeability $k_{Cap} = 10^{-19}$ m^2, above (cap rock) and below the target 100 m thick sandstone reservoir, with permeability $k_{Aq} = 10^{-13}$ m^2. The system is considered isothermal, with temperature and pressure gradients respectively of 25 ^{o}C km^{-1} and 9.81 MPa km^{-1}. The horizontal and vertical permeabilities of rock units and of the fault gouge at different layers are assumed equal; other rock and fault characteristics are given in Table 1. On the fault plane, the permeability in the sandstone section is $k_{F\text{-}Aq}$ while in the shale sections it is $k_{F\text{-}Cap}$. A positive difference between $k_{F\text{-}Aq}$ and $k_{F\text{-}Cap}$ equal to or greater than two orders of magnitude makes the fault in the sand hydraulically invisible from the injection well (i.e., it does not represent a flow barrier): under these conditions, the CO_2/brine flow may easily cross the fault with minimal pressure gradient across its surface. Thus fault slip and consequent energy release do not occur. For our reference case, values of fault permeability were $k_{F\text{-}Aq} = 10^{-15}$ m^2 in the fault gauge of the sandstone and $k_{F\text{-}Cap} = 10^{-16}$ m^2 in the fault gauge of the shale.

The CO_2 is injected with a constant injection rate of 0.02 kg s^{-1} m^{-1} (Figure 6), similarly to previous studies (e.g. Rutqvist et al., 2007, 2008; Cappa & Rutqvist, 2011b). The computational domain was set open to fluid flow, except for the left boundary where no flow conditions were set. The left boundary was constrained to allow displacements in the vertical direction only, while the bottom boundary was constrained to allow displacements in the horizontal direction only (Figure 6).

We made two sets of runs. In the first set, permeability values were decreased from the reference case to $k_{F\text{-}Aq} = 10^{-16}$ m^2 and $k_{F\text{-}Cap} = 10^{-17}$ m^2, and to $k_{F\text{-}Aq} = 10^{-17}$ m^2 and $k_{F\text{-}Cap} = 10^{-18}$ m^2. In the second set, we kept permeability values at the reference-case value, varying the ratio of horizontal to vertical stresses (σ_H/σ_V), which describes the state of stress in the model volume, from 0.7 in the reference case, to the values of 0.67 and 0.65, in order to

consider changes in stress conditions at the fault surface. This is practically equivalent to varying the dip of the fault or, in a 3D geo-mechanic environment, to considering normal faults whose plane is not parallel to σ_2. In our 2D simulations, in which the fault is not allowed to have any strike-slip component of strain, this situation may represent the stress conditions on a fault plane, created as a response to an older stress field, and not favorably oriented for reactivation in the current stress field.

Results of the simulations quantify the amount of seismic energy released by the slipping fault and are represented in Figures 7 and 8, in terms of pore-pressure changes and amounts of slip for the two cases considered in each set of trials, plus the reference case. In the first series of runs (Figure 7), only a fraction of the fault surface is subject to slip in proximity of the contact between cap rock and aquifer. Over the range of fault permeability considered, results indicate no significant impact of permeability on fault slip, stress drop, and energy release, but do show variations in the timing of rupture. These scenarios may generate seismic events with a magnitude of about 2.7.

The second set of simulations considers changes in stress ratio (σ_H/σ_V), as shown in Figure 8. The results indicate that different amounts of pressure buildup can exist long before slippage occurs for different stress-conditions at the fault surface (Figure 8a). Also, the magnitude of slip and rupture length involved depends on the stress ratio, with larger events triggered for smaller ratios (Figure 8b). In the worst-case simulated scenario, magnitude reached a maximum value of 3.63, consistent with the one calculated using empirical relations (Equation 4) and with the assumption of rupture extending over the entire fault length.

Figure 9 represents conditions of shear stress and shear strength immediately before and after the slip on the fault plane (for simplicity, only the reference case is shown). Shear strength is reduced by the increased pore pressure, resulting in a minimum value at the top

of the reservoir. The shear stress also changes before failure across the thickness of the aquifer (Figure 9b, blue line). These changes are caused by poroelastic effects occurring within the aquifer, as the pressure increases (i.e., reservoir swelling). The sum of the two effects results in a rupture that nucleates at the bottom of the reservoir.

5 Discussion

The first set of simulations suggests that the maximum amount of pressure buildup (reduction of shear strength) that can be sustained by a fault before slippage is related to its permeability: high values of $k_{F\text{-}Aq}$ do not allow for pressure buildup, inhibiting fault reactivation. Differences in values of aquifer and cap-rock permeability, though, do not affect the extent of fault surface undergoing slippage and the consequent magnitude of the event).

The second set of simulations illustrates how the maximum earthquake magnitude caused by undetected faults depends on the geometrical relationships between the fault and the principal stresses, for any given geological condition. From Figure 8, it is clear how, in our 2D simulations, a fault which is not favorably oriented for reactivation would stand a higher value of pressure buildup accumulation and, when slipping, would accommodate less strain, thus releasing less energy.

Analogously to oil traps (e.g., Finkbeiner et al., 2001), the transmissivity of a fault and its state of stress control the thickness of the CO_2/brine column that could accumulate under the cap rock-fault plane trap. This thickness is proportional to the maximum pressure buildup that could eventually develop on the fault plane, before the fault ruptures and slips.

When undetected faults (e.g., faults with $D \leq 10$ m) intersect a sand reservoir (where SGR < 0.15) interbedded within shales (with SGR > 0.4), the low permeability (transmissivity) of the fault plane within the sandstone may be limited to its upper and lower parts (~10 m), where the clay minerals (phyllosilicates) are smeared onto the sand along the fault contact - even though the overall transmissivity of the fault could still remain relatively high and little

pressure build up could occur. However, for critically stressed faults, the pressure buildup on the upper part of the fault plane through the target reservoir may be enough to cause fault rupture and slip along its entire surface. Therefore, the maximum magnitude of the induced earthquake is limited by fault length (about 1 km for our case), to a value of about 3.6. While this would not be considered a major earthquake and probably would not cause significant damage to surface structures, it would likely alarm the local population, if the GCS injection is located sufficiently near an inhabited area. In addition, over a longer time scale, the enhanced permeability along the fault planes, during active phases, could impact the performance of a sequestration project, allowing for CO_2/brine leakage and potentially affecting the surface environment. It should be noted that shallower Underground Sources of Drinking Water (USDW, Oldenburg et al., 2009) may not be intersected by small, undetected faults which cut the storage reservoir near the middle of their length (as in our simulations). Consequently they may not be susceptible to contamination from stored CO_2 or brine.

6 Conclusions

- Faults can be leakage paths for fluids from inside the Earth's crust. In accordance with the concepts of fault' valve behavior (Sibson, 1990) and periodic fluid flow along faults (Hooper, 1991), the vertical permeability of a fault plane through a shale cap rock is dependent on its stress conditions and on the total amount of pressure that can accumulate on the fault, for given stress conditions - which in turn is a function of fault transmissivity. The potential for a fault to become conductive to flow during periods of activity can account for gas anomalies sometimes recorded near fault outcrops before large natural seismic event (e.g., L'Aquila 2009). In spite of their limited extents and throws, minor undetected faults can act as baffles to fluid flow and become sites of pressure buildup, with the potential for consequent release of seismic energy. Precise

characterization of target aquifers is of importance for GCS, both in terms of induced seismicity potentials and efficiency of the sequestration system (lack of leakage).

- The maximum magnitude of an earthquake generated by a fault which is small enough (e.g., 1 km length, as considered in this study) to be undetected by current surface geophysical investigations and caused by pore pressure increase due to CO_2 injection is unlikely to be characteristic of a major event ($7 < M < 7.9$), but rather of a minor event ($2 < M < 3.9$);
- Minor faults considered in this research have a limited extent and probably would not reach upward all the way to Underground Sources of Drinking Water (USDW). In addition, these faults would not cut a thick (e.g., > 500 m) cap rock through its entire thickness.

ACKNOWLEDGEMENTS

The work presented in this paper was financed by the Assistant Secretary for Fossil Energy, Office of Natural Gas and Petroleum Technology, through the National Energy Technology Laboratory, under the U.S. Department of Energy Contract No. DE-AC02-05CH11231. Technical reviews by Curt Oldenburg, Tom Daley and Ernie Majer, as well as editorial review by Dan Hawkes, Lawrence Berkeley National Laboratory are all greatly appreciated. We would also like to thank two anonymous reviewers whose comments and suggestions improved the work considerably.

References

Abercrombie, R.E., 1995, Earthquake source scaling relationships from -1 to 5 using seismograms recorded at 2.5-km depth: Journal of Geophysical Research, v. 100, p. 24,015-24,036. doi: 0148-0227/95/95JB-02.

Antonellini & Aydin, 1994. Effects of faulting on fluid flow in porous sandstones: petrophysical properties. AAPG Bulletin, v. 78, pp. 181-201

Barton, C.A., Zoback, M.D., Moos, D., 1995. Fluid flow along potentially active fault in crystalline rock. Geology, v. 23, pp.683-686

Bath, M., 1981, Earthquake Magnitude - recent researh and current trends: Earth-Science Reviews, v. 17, pp. 315-398. doi: 0012-8252/81/0000--0000.

Birkholzer, J.T., & Zhou, Q., 2009, Basin-scale hydrogeologic impacts of CO_2 storage: Capacity and regulatory implications: International Journal of Greenhouse Gas Control, v. 3, pp. 745-756. doi:10.1016/j.ijggc.2009.07.002.

Birkholzer, J.T., Nicot, J.P., Oldenburg C.M., Zhoua, Q., Kraemer, S., Bandilla, K., 2011, Brine flow up a well caused by pressure perturbation from geologic carbon sequestration: Static and dynamic evaluations. Int. J. Greenhouse Gas Control. v. 5 (4), pp. 850-861, doi: doi:10.1016/j.ijggc.2011.01.003

Bouvier, J.D., Kaars-Sijpesteijn, C.H., Kluesner, D.F., Onyejekwe, C.C., Van der Pal, R.C., 1989. Three-dimensional seismic interpretation and fault sealing investigations, Nun River Field, Nigeria. AAPG Bulletin, v. 73, pp. 1397-1414, doi:10.1306/44B4AA5A-170A-11D7-8645000102C1865D

Cappa, F. & Rutqvist, J., 2011(a), Impact of CO_2 geological sequestration on the nucleation of earthquakes, Geophysical Research Letter, v. 38, L17313, doi:10.1029/2011GL048487 (2011).

Cappa, F. & Rutqvist, J., 2011(b), Modeling of coupled deformation and permeability evolution duting fault reactivation induced by deep underground injection of CO_2. Int. J. Greenhouse Gas Control, v. 5, (2011), doi:10.1016/j.ijggc.2010.08.005

Chavez-Perez, S., & Louie, J.N., 1997, Seismic reflection views of the 1994 Northridge earthquake hypocentral region using aftershock data and imaging techniques: Reno, NV, Seismological Laboratory, Mackat School of Mines, University of Nevada, http://crack.seismo.unr.edu/htdocs/students/CHAVEZ/curee97/curee97.pdf.

Childs, C., Walsh, J.J., Manzocchi, T., Bonson, C. Nicol, A., Schopfer, M.P.J., 2009. A geometric model of fault zone and fault rock thickness variations. J. Structural Geology, v. 31, pp. 117-27 doi:10.1016/j.jsg.2008.08.009.

Chyi, L.L., Quick, T.J., Yang, T.F. & Chen, C.-H., 2005. Soil Gas Radon Spectra and Earthquakes. Terr. Atmos. Ocean. Sci., V. 16 (4), pp. 763-774. http://tao.cgu.org.tw/index.php?id=707

Cowie, P., and Scholz, C.H., 1992, Displacement-length scaling relationship for faults: data synthesis and discussion: J. Structural Geology, v. 14, pp. 1149-1156. doi: 0191-8141/92.

Court, B., 2011. Safety and Water Challenge in CCS: Modelling Studies to Quantify CO_2 and Brine Leakage Risk and Evaluate Promising Synergies for Active and Integrated Water Management. Ph.D. thesis, Princeton University. September 2011..

Court,B., Celia, M.A., Nordbotten, J.M., Dobossy, M., Elliot, T.R., Bandilla, K.W., 2011. Modeling options to answer practical questions for CO_2 Sequestration operations. Manuscript available at: http://arws.princeton.edu/ark:/88436/dsp01rf55z769f

Dannwolf, U.S. & Ulmer, F., 2009. AP6000 Report: Technology Risk Comparison of the Geothermal DHM Project in Basel, Switzerland - Risk Appraisal including Social Aspects. RC006. http://www.google.com/url?sa=t&rct=j&q=&esrc=s&source=web&cd=8&ved=0CFgQFjAH&url=http%3A%2F%2Fwww.wsu.bs.ch%2Fserianex_appendix_5.pdf&ei=w6oxT-PhBof9iQLy7PWMCg&usg=AFQjCNGIJ9B-x48ot75EhfhS-tD5m62vUA

Dawers, N.H., Anders, M.H., and Scholz, C.H., 1993, Growth of normal faults: displacement-length scaling. Geology, v. 21, pp. 1107-1110.

Dost, B., & Haak, H.W., 2007, Natural and induced seismicity, in Wong, T.E., Batjes, D.A.J., and de Jager, J., eds., Geology of the Netherlands.

Dowrick, D.J., & Rhoades, D.A., 2004, Relations Between Earthquake Magnitude and Fault Rupture Dimensions: How Regionally Variable Are They?: Bulletin of the Seismological Society of America, v. 94, pp. 776–788.

EERI, 2009, The Mw 6.3 Abruzzo, Italy, Earthquake of April 6, 2009. Report funded by the Earthquake Engineering Research Institute, Learning from Earthquakes project, under grant #CMMI-0758529, National Science Foundation. http://www.eeri.org/site/images/lfe/pdf/laquila-eq-report.pdf

Ferrill, D.A., Smart, K.J., and Necsoiu, M., 2008, Displacement-length scaling for single-event fault ruptures: insights from Newberry Springs Fault Zone and implications for fault zone structure, in Wibberley, C.A.J., Kurz, W., Imber, J., Holdsworth, R.E., and Collettini, C., eds., The Internal Structure of Fault Zones: Implications for Mechanical and Fluid-Flow Properties: London, The Geological Society of London. DOI: 10.1144/SP299.7.

Ferrill, D.A. & Morris, A.P., 2003. Dilational normal faults. J. Structural Geology, v. 25, pp. 183-196, doi:10.1016/S0191-8141(02)00029-9

Finkbeiner, T., Zoback, M.D., Flemings, P., 2001. Stress, pore pressure and dynamically constrained hydrocarbon columns in the South Eugene Island 330 field, northern Gulf of Mexico. AAPG Bulletin, v. 85, pp. 1007-1031

Friedmann, H., 2011. Radon in Earthquake Prediction Research. J. of Radiation Protection Dosimetry (2011), pp. 1-8; doi: 10.1093/rpd/ncr229

Gauthier, B.D.M., & Lake, S.D., 1993, Probabilistic modeling of faults below the limit of seismic resolution in Pelican Field, North Sea, offshore United Kingdom. AAPG Bulletin, v. 5, pp. 761-777.

Giampiccolo, E., D'Amico, S., Patane`, D., and Gresta, S., 2007, Attenuation and Source Parameters of Shallow Microearthquakes at Mt. Etna Volcano, Italy. Bulletin of the Seismological Society of America, v. 97, pp. doi: 10.1785/0120050252.

Gupta, A., & Scholz, C.H., 2000, A model of normal fault interaction based on observations and theory: J. Structural Geology, v. 22, pp. 865-879. PII: S0191-8141(00)00011-0.

Hanks, T.C., & Kanamori, H., 1979, A Moment Magnitude Scale: Journal of Geophysical Research, v. 84, p. 2348-2350. doi: 0148-0227/79/009B-0059.

Hesthammer, J. & Fossen, H., 1997. Seismic attribute analysis in structural interpretation of Gullfaks Field, northern North Sea. Petroleum Geoscience, v. 3, pp.13-26. doi: 10.1144/petgeo.3.1.13.

Hooper, E.C.D., 1991. Fluid migration along growth faults in compacting sediments. J. Petr. Geology, v. 14(2), pp. 161-180

Iida, K., 1959, Earthquake energy and earthquake fault. J. Earth Science. Nagoya University, v. 7, pp. 98-107.

Kanamori, H., 1977. The Energy Released by Great Earthquakes. J. Geophysical Research, v. 82(20), pp. 2981-2988.

Kim, S.Y., & Sanderson, D.J., 2005, The relationship between displacement and length of faults: a review: Earth Science Reviews, v. 68, pp. 317 - 334. doi:10.1016/j.earscirev.2004.06.003.

Kumar, A.S., Singh, S., Mahajan, S., Bajwa, B.S., Kalia, R. & S. Dhar, 2009. Earthquake precursory studies in Kangra Valley, North-East Himalayas, India, with special enphasis on radon emission. Appl. Radiat. Isot., v. 67, pp. 1904-1911, doi: 10.1016/j.apradiso.2009.05.016.

Majer, E.L., Baria, R., Stark, M., Oates, S., Bommer, J., Smith, B., Asanuma, H., 2007. Induced seismicity associated with Enhanced Geothermal Systems. Geothermics, v. 36, pp. 185-222. doi:10.1016/j.geothermics.2007.03.003

Manzocchi, T., Walsh, J.J., Nell, P., Yielding, G., 1999. Fault transmissibility multipliers for flow simulation models. Petroleum Geoscience, v. 5. Geological Society, London; doi:1354-0793/99.

Manzocchi, T., Childs, C., Walsh, J.J., 2010. Faults and fault properties in hydrocarbon flow models. Geofluids (2010) v. 10, pp 94-113; doi:10.1111/j.1468-8123.2010.00283.x

Mazzoldi, A., 2004, Hydrogeochemical studies of Val Caffarella. Studies of crustal/magmatic origin of the gas CO_2 found in water of the river Almone, district of the Alban Hills, Rome (I), through the determination of the activity of the radioactive gas Radon-222. M.S. thesis (Italian), University of Roma Tre, unpublished work.

McGarr, 1976. Seismic Moments and Volume Changes. Journal of Geophysical Research. V. 81 (8), pp. 1487-1494

Morris, A.P., Ferril, D.A., and Henderson, D.B., 1996, Slip tendency analysis and fault reactivation. Geology, v. 24, pp. 275-278. DOI: 10.1130/0091-7613(1996)024<0275.

Morris, A.P., Ferril, D.A., McGinnis, R.N., 2010. Fault frequency and strain. Litosphere (2009) v. 1, pp. 105-109; doi:10.1130/L23.1

Nicot, J.P., 2008. Evaluation of large-scale CO_2 storage on fresh-water sections of aquifers: An example from the Texas Gulf Coast Basin. Int. J. Greenhouse Gas Control, v. 2, pp. 582-593. doi:10.1016/j.ijggc.2008.03.004

Oldenburg, C.M., 2007.Migration mechanisms and potential impacts of CO_2 leakage and seepage, in Wilson and Gerard, editors, Carbon Capture and Sequestration Integrating Technology, Monitoring, and Regulation, pp 127-146, Blackwell Publishing 2007.

Oldenburg, C.M., S.L. Bryant, and J.-P. Nicot, Certification Framework Based on Effective Trapping for Geologic Carbon Sequestration, Int. J. of Greenhouse Gas Control, v. 3, (4), pp.445–457, 2009, LBNL-1549E.

Oldenburg, C.M. & J.T. Birkholzer, 2010. Comparative Assessment of Status and Opportunities for CO_2 Capture and Storage and Radioactive Waste Disposal in North America, Internal Report, Lawrence Berkeley National Laboratory. LBNL Paper LBNL-3492E. http://escholarship.org/uc/item/82k795t3#page-1

Oldenburg, C.M. & A.P. Rinaldi, 2011, Buoyancy Effects on Upward Brine Displacement Caused by CO_2 Injection, Transp. Porous Media, v. 87, pp. 525-540

Pals, F., 2010, Shell's Barendrecht Carbon-Capture Project Canceled, Bloomberg Businessweek, Bloomnerg, http://www.businessweek.com/news/2010-11-04/shell-s-barendrecht-carbon-capture-project-canceled.html.

Pruess, K., 2003, Numerical simulation of leakage from a geologic disposal reservoir for CO_2, with transitions between super- and sub-critical conditions, TOUGH Symposium 2003: Lawrence Berkeley National Laboratory Berkeley, CA, May12–14.

Richon, P., Klinger, Y., Tapponnier, P., Li, C.-X., Van Der Woerd, J., Perrier, F., 2010, Measuring Radon fluxes accrross active faults: Relevance of excavating and possibility of satellite discharges. Int. J. Radiation Measurements, v. 45 (2010), pp. 211–218; doi:10.1016/j.radmeas.2010.01.019

Rutqvist, J., Wu, Y.-S., Tsang, C.-F., Bodvarsson, G., 2002. A modeling approach for analysis of coupled multiphase fluid flow, heat transfer, and deformation in fractured porous rock. Int. J. Rock Mech. Min. Sci. v. 39, pp. 429-442

Rutqvist, J., Birkholzer, J., Cappa, F., and Tsang, C.-F., 2007, Estimating maximum sustainable injection pressure during geological sequestration of CO_2 using coupled fluid flow and geomechanical fault-slip analysis: Energy Conversion and Management, v. 48, pp. 1798–1807. doi:10.1016/j.enconman.2007.01.021.

Rutqvist, J., Birkholzer, J.T., and Tsang, C.F., 2008, Coupled Reservoir-Geomechanical Analysis of the Potential for Tensile and Shear Failure Associated with CO_2 Injection in Multilayered Reservoir-Caprock system: Int. J. Rock Mech. & Min. Sci, v. 45, pp. 132-143. doi:10.1016/j.ijrmms.2007.04.006.

Rutqvist, J., & Stephansson, O., 2003, The role of hydromechanical coupling in fractured rock engineering: Hydrogeology Journal, v. 11, pp. 7-40.

Rutqvist, J., 2012. The geomechanics of CO_2 storage in deep sedimentary formations. International Journal of Geotechnical and Geological Engineering; doi:10.1007/s10706-011-9491-0.

Schlische, R.W., Young, S.S., Ackermann, R.V., and Gupta, A., 1996, Geometry and scaling relations of a population of very small rift-related normal faults: Geology, v. 24, pp. 683-686. doi: 10.1130/0091-7613.

Schultz, R.A. & Fossen, H., 2002, Displacement–length scaling in three dimensions: the importance of aspect ratio and application to deformation bands: Journal of Structural Geology, v. 24, pp. 1389–1411. PII: S0191-8141(01)00146-8.

Shapiro, S.A., Dinske, C., and Kummerow, J., 2007, Probability of a given-magnitude earthquake induced by a fluid injection: Geophysical research letters, v. 34, pp. doi:10.1029/2007GL031615.

Shapiro, S.A., Dinske, C., and Langenbrugh, C., 2010, Seismogenic index and magnitude probability of earthquakes induced during reservoir fluid simulations. Society of Exploration Geophysicists (The leading Edge). 2010 v. 29 (3) pp. 304-309. doi: 10.1190/1.3353727..

Shaw, B.E., 2009, Constant Stress Drop from Small to Great Earthquakes in Magnitude-Area Scaling: Bulletin of the Seismological Society of America, v. 99, pp. 871-875, doi: 10.1785/0120080006.

Sibson, R.H., 1990. Conditions for fault-valve behavior. Geological Society, London, Special Publications, 1990, v. 54, pp. 15-28.

Singh, S., Kumar, A., Bajwa, B.S., Mahajan, S., Kumar, V. & Dhar, S., 2009. Radon Monitoring in Soil Gas and Ground Water for Earthquake Prediction Studies in North-West Himalayas, India. Terr. Atmos. Ocean. Sci., v. 21 (4), pp. 685-695. doi: 10.3319/TAO.2009.07.17.01(TT).

Smith, D.A., 1966, Theoretical considerations of sealing and non-sealing faults. AAPG Bull., v. 50 (2), pp. 363-374.

Talwani, P., Moore, W.S. & Chiang, J., 1980. Radon anomalies and microearthquakes at Lake Jocassee, South Carolina, J. Geophys. Res., v. 85. pp. 3079-3088; doi: 10.1029/JB085iB06p03079.

Terzaghi, K. and Peck, R. B. (1948). Soil Mechanics in Engineering Practice. John Wiley and Sons, New York; Chapman and Hall, London.

Torabi, A. & Berg, S.S., 2011. Scaling of fault attribute: a review. Marine and Petroleum Geology, v. 28, pp. 1444-1460. doi: 10.1016/j.marpetgeo.2011.04.003.

Ulomov, V.I. & Mavashev, B.Z., 1967. A precursor of a strong tectonic earthquake. Acad. Sci. USSR Earth Sci. Sect. 176, 9-11.

Wells, D.L., & Coppersmith, K.J., 1994, New Empirical Relationships among Magnitude, Rupture Length, Rupture Width, Rupture Area, and Surface Displacement: Bulletin of the Seismological Society of America, v. 84, pp. 974-1002.

Yielding, G., Freeman, B., Needham, D.T. 1997. Quantitative fault seal prediction. AAPG Bulletin, v. 81(6), pp. 897-917; doi: 10.1306/522B498D-1727-11D7-8645000102C1865D.

Yielding, G., Bretan, P., Freeman, B., 2010. Fault seal calibration: a brief review. Geological Society, London, Special Publications, v. 347, pp. 243-255. Doi:10.1144/SP347.14.

Zhou, Q. & Birkholzer, J.T., 2010. On scale and magnitude of pressure build-up induced by large-scale geologic storage of CO_2. Greenhouse Gas Sci Technol., v. 1 (1), pp 11–20 (2011); DOI: 10.1002/ghg3

Zoback, M.D. & Zinke, J.C., 2002. Production-induced Normal Faulting in the Valhall and Ekofisk Oil Fields. Pure and Applied Geophysics, v. 159, pp. 403-420; doi:0033-4553/02/030403-18

Table

Table 1. Rock characteristics considered in the simulations

Parameters	**Storage Aquifer**	**Cap rock**	**Upper Aquifer**	**Basal Aquifer**	**Fault**
Young's modulus, E (GPa)	10	10	10	10	5
Poisson's ratio, ν (-)	0.25	0.25	0.25	0.25	0.25
Rock density, ρ_s (kg/m^3)	2260	2260	2260	2260	2260
Biot's coefficient, α (-)	1	1	1	1	1
Friction angle, φ (°)	-	-	-	-	25
Dilation angle, ψ (°)	-	-	-	-	20
Porosity, ϕ (-)	0.1	0.01	0.1	0.01	0.1
Permeability, k (m^2)	1×10^{-13}	1×10^{-19}	1×10^{-14}	1×10^{-16}	Variable (see text)
Residual gas (CO_2) saturation (-)	0.05	0.05	0.05	0.05	0.05
Residual liquid saturation (-)	0.3	0.3	0.3	0.3	0.3
Van Genuchten (1980), P_0 (kPa)	19.9	621	19.9	621	19.9
Van Genuchten (1980), m (-)	0.457	0.457	0.457	0.457	0.457

Figure

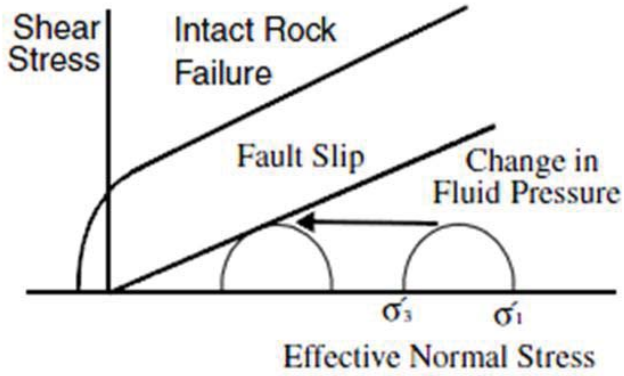

Figure 1. A simple and efficient method for determining the stability of a rock: the Mohr circle and the effective stress law relates fluid pressure to regional stresses acting on a fault and to the limit for slippage. An increase in pore pressure can cause slip along pre-existing faults by reduction of the effective normal stress on the fault plane.

Figure

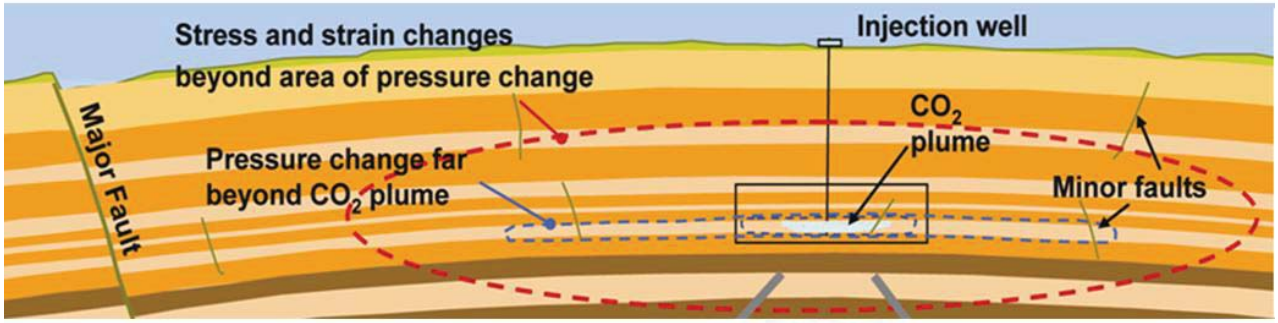

Figure 2. Schematic representation of a domal structure which is being used for CO_2 sequestration. Note the difference in extension between the plume of the injected CO_2, the pressure buildup and potential interactions with major and minor faults (Rutqvist, 2012).

Figure

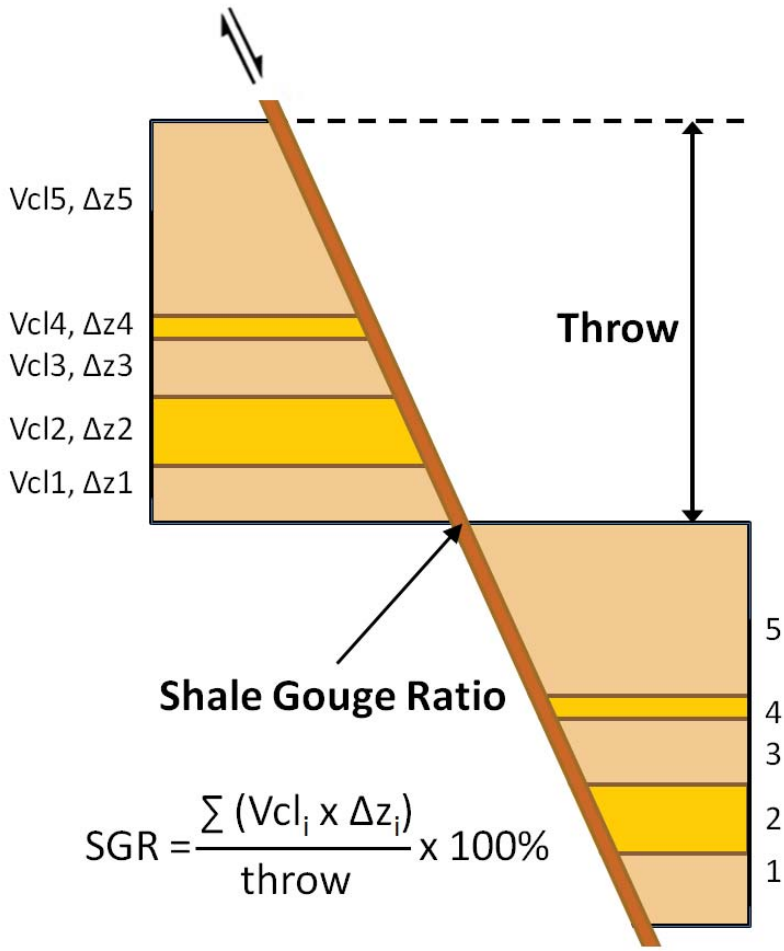

Figure 3. A schematic representation of Shale Gouge Ratio, as conceptualized by exploration geologists. Image modified from Yielding et al. (2010)

Figure

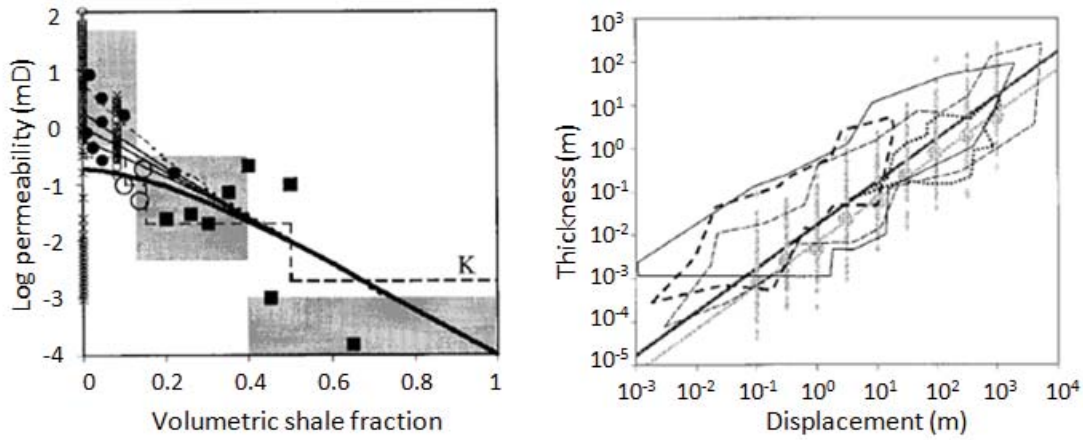

Figure 4. The two graphs relate a) across-fault permeability to SGR and b) fault-zone thickness to displacement. Data are from a variety of locations (Figure 2 in Manzocchi et al., 1999). Also plotted are synthetic values generated using Equation 2 for permeability and the relation $t_F = D/66$ to define a median fault gouge thickness value (Manzocchi et al., 1999).

Figure

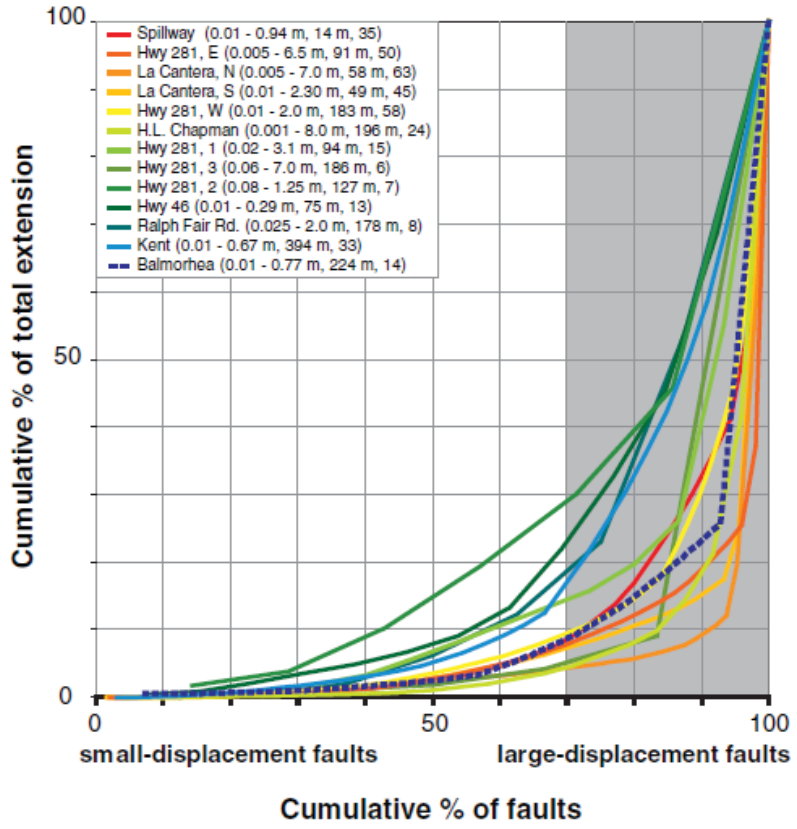

Figure 5. Fault displacement distribution plotted as cumulative fault contribution to total extensional strain, normalized by total extensional strain. Shaded area represents largest 30% of total fault population (Morris et al., 2010).

Figure

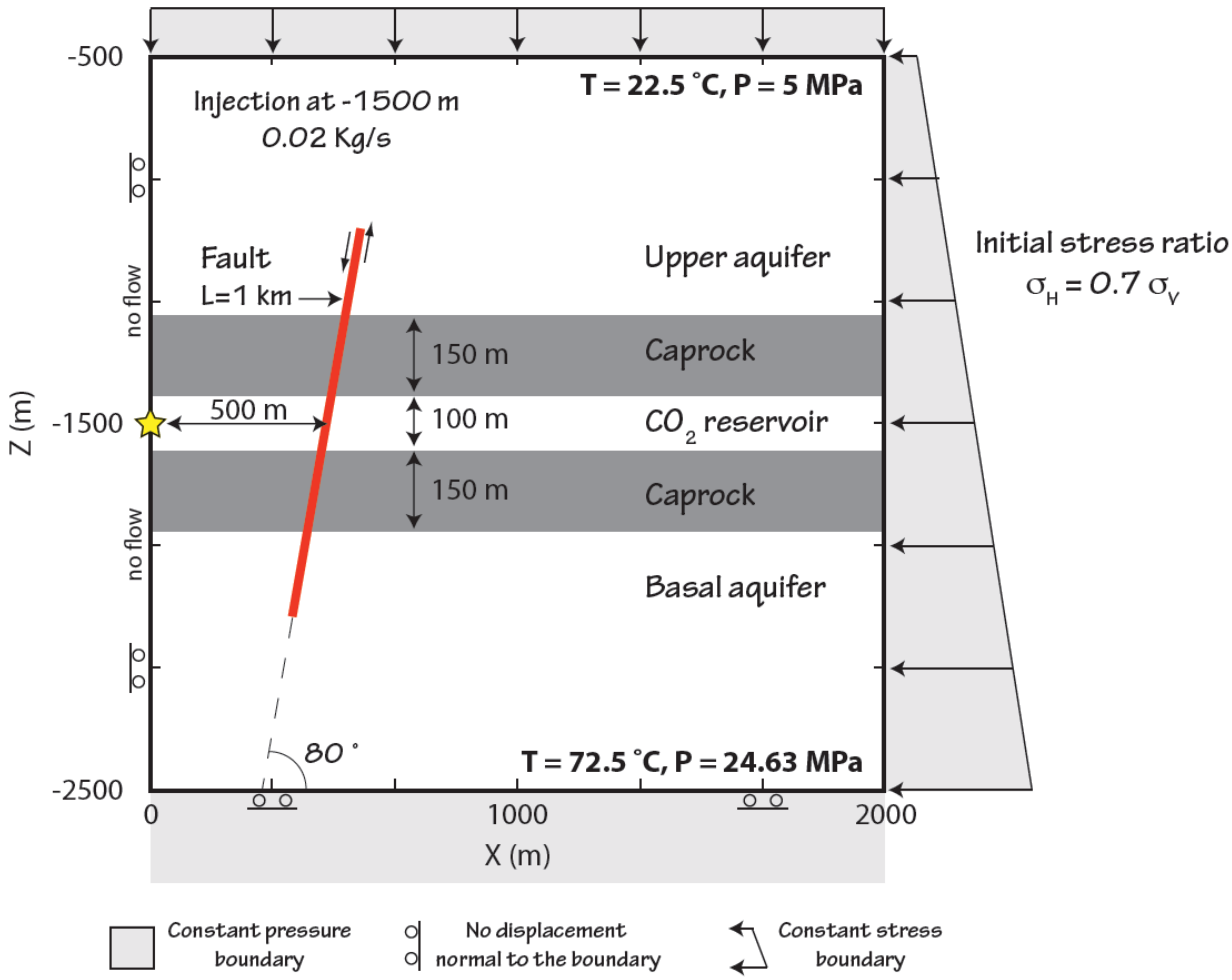

Figure 6. The modeled hydro-mechanical environment, which includes a blind fault with a $D_{MAX} \leq 10$ m (undetected by geophysical surveys, and too small to be visible in the figure). The star shows the injection point.

Figure

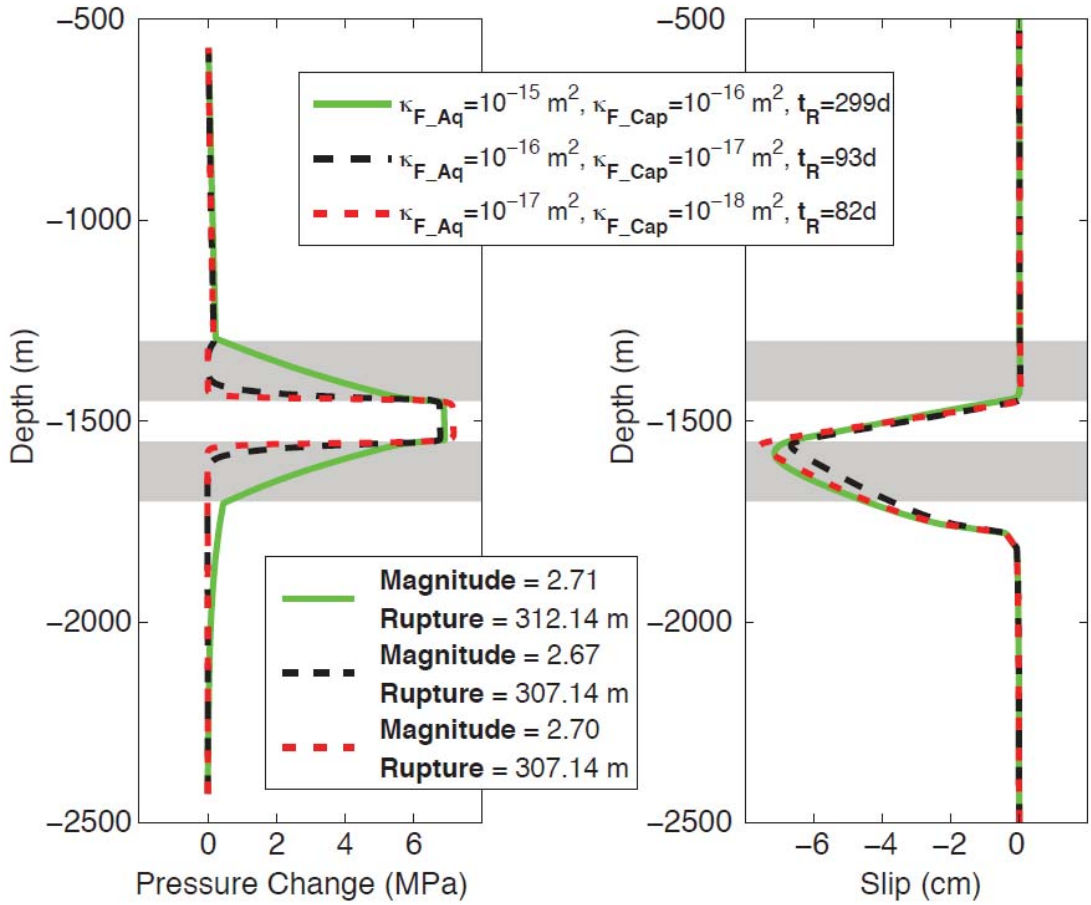

Figure 7. Results of pressure change and slip amount of the fault walls in simulations with TOUGH-FLAC, for the fault considered. The different curves represent different values of $k_{F\text{-}Aq}$ and $k_{F\text{-}Cap}$ at the fault surface. Reported are values for length of slipping ruptures, magnitude of the seismic events generated, and time (t_R) at which the rupture occurs. "Rupture" is the length of fault rupture in [m].

Figure

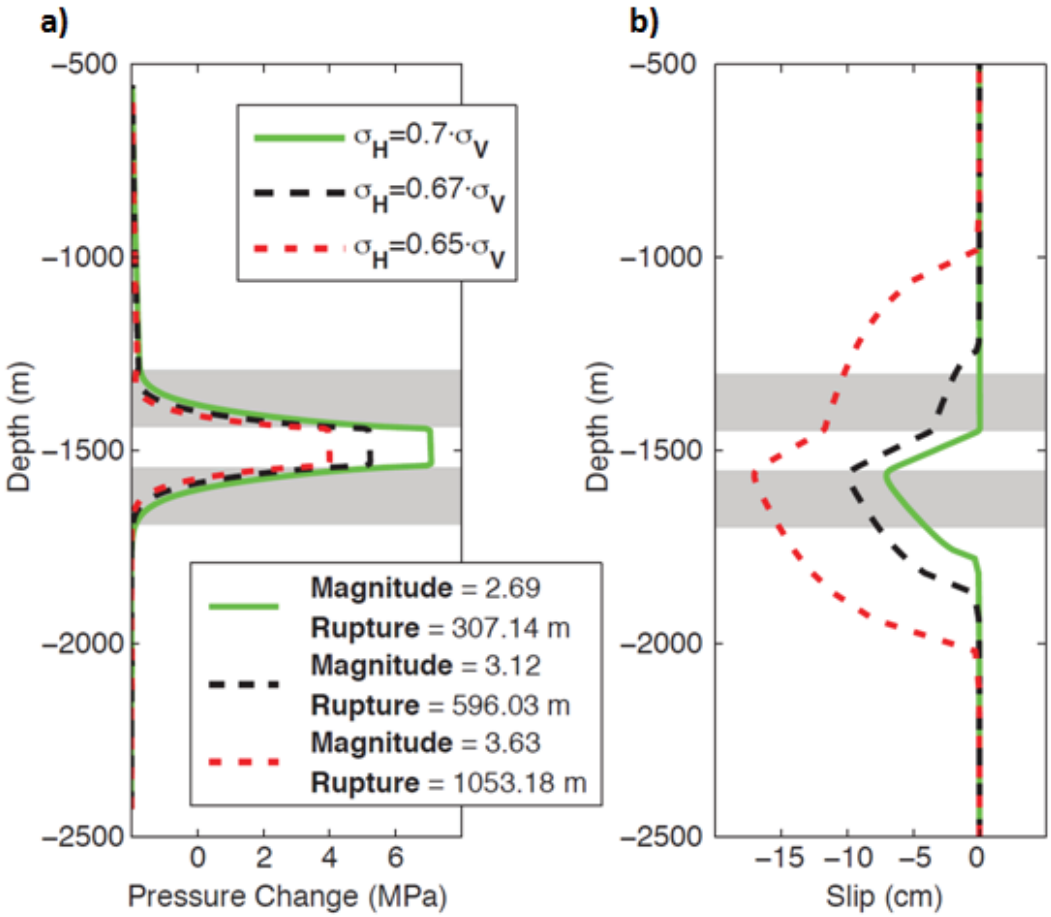

Figure 8. Results of simulations analyzing the response of fault slip to changes in value of stress at the fault surface, considering ratios σ_H/σ_V equal to 0.7 (Base case), 0.67 and 0.65. Highest resulting values are for faults nearest to critical-stress state. Values of length of the rupture involved in the slip and consequent energy released are also reported, [m].

Figure

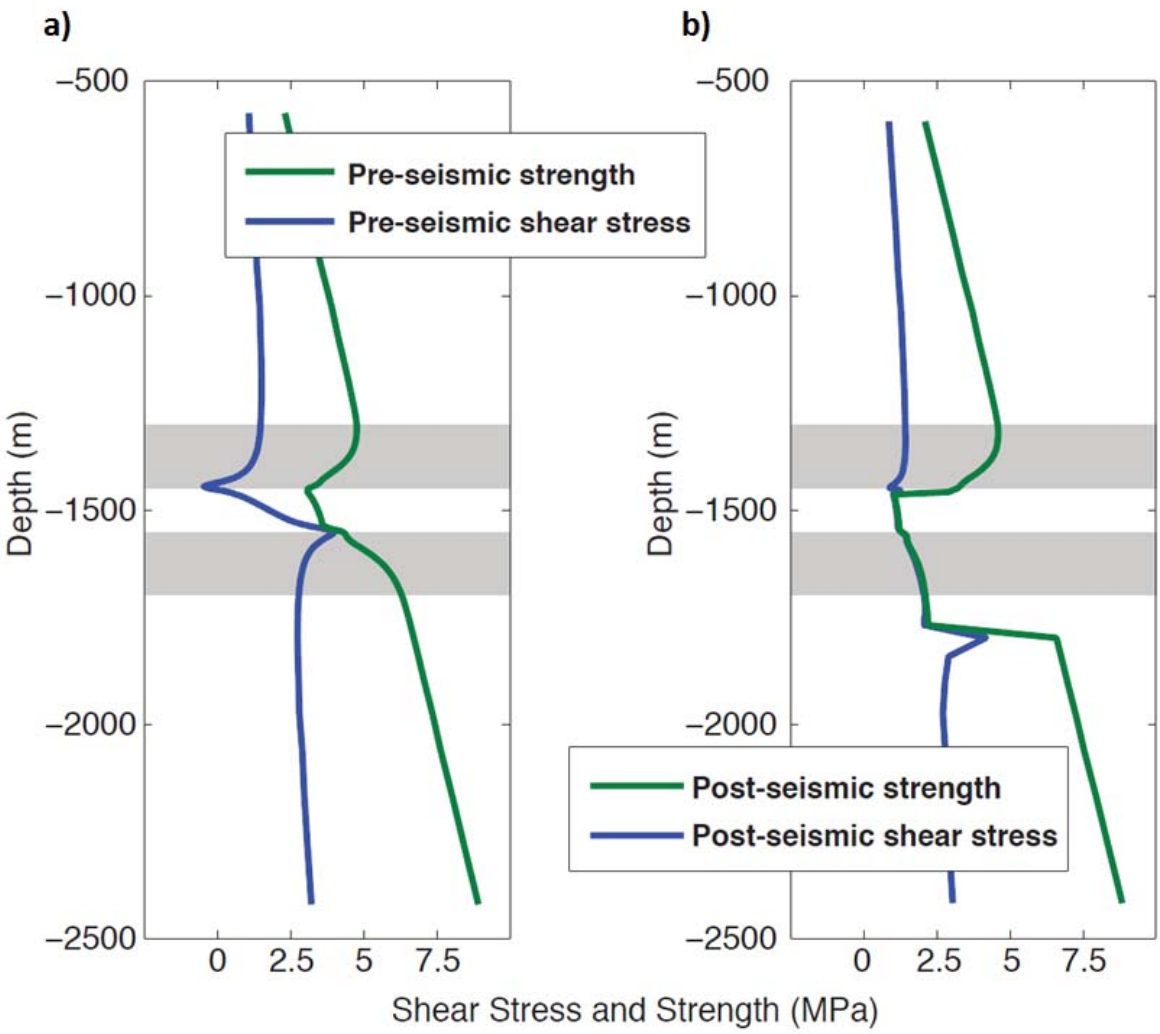

Figure 9. (a) Pre- and (b) post-seismic stress conditions at the fault surface during GCS operations.

DISCLAIMER

This document was prepared as an account of work sponsored by the United States Government. While this document is believed to contain correct information, neither the United States Government nor any agency thereof, nor The Regents of the University of California, nor any of their employees, makes any warranty, express or implied, or assumes any legal responsibility for the accuracy, completeness, or usefulness of any information, apparatus, product, or process disclosed, or represents that its use would not infringe privately owned rights. Reference herein to any specific commercial product, process, or service by its trade name, trademark, manufacturer, or otherwise, does not necessarily constitute or imply its endorsement, recommendation, or favoring by the United States Government or any agency thereof, or The Regents of the University of California. The views and opinions of authors expressed herein do not necessarily state or reflect those of the United States Government or any agency thereof or The Regents of the University of California.

Ernest Orlando Lawrence Berkeley National Laboratory is an equal opportunity employer.